BULLETIN OF THE POLISH ACADEMY OF SCIENCES
TECHNICAL SCIENCES, Vol. 70(3), 2022, Article number: e141181
DOI: 10.24425/bpasts.2022.141181

Stress and strain distribution in X10CrMoVNb9-1 power engineering steel after long time degradation studied by the ESPI system

Mateusz KOPEC*

Institute of Fundamental Technological Research, Polish Academy of Sciences, Pawinskiego 5B, 02-106 Warsaw, Poland and
Department of Mechanical Engineering, Imperial College London, London SW7 2AZ, UK

Abstract. Maintenance of assets and equipment in power plants is essential for their safety and is required to help the plant stay active. In this paper, the specimens manufactured from a pipe of X10CrMoVNb9-1 (P91) power engineering steel in the as-received state and after operating for 80 000 h at internal pressure of 8.4 MPa and temperature of 540ºC were subjected to tests using electronic speckle pattern interferometry (ESPI) under static loading of up to 2.5 kN. Such a procedure enables assessment of strain and stress distribution maps to compare material integrity in the as-received state and after exploitation in its elastic range. The measurements conducted showed no effect of long time operation on the mechanical response of P91 steel under the power installations conditions since the field strain distributions for each type of specimen were found to be similar.

Key words: damage; P91 steel; electronic speckle pattern interferometry (ESPI); optical measurements.

1. INTRODUCTION

With the increasing demands of the power industry, the high efficiency of equipment and working machines has become a dominant issue that engineers are trying to improve. In most recent decades, the operating parameters of power plant elements differ significantly from their counterparts used in the past. At the beginning of the 20th century, the operating temperature was 370°C, while internal pressure was close to 4 MPa. In recent years, supercritical parameters increased significantly, to 620°C and 30 MPa, accordingly. In addition, ambitious plans to minimize the impact of power plants on the environment by reduction of CO_2 have been put forward. Industry engineer groups together with scientists are constantly working on new construction materials that could be used responsibly under extreme operating conditions. P91 (X10CrMoVNb91) [1] and P92 (X10CrWMoVNb9-2) steels [2], and others such as P22 (10CrMo9-10) [3] and VM 12 (X12CrCoWVNb12-2-2) [4] can be distinguished among these materials. As compared to earlier steels used in the power plant sector, these materials are characterized by higher mechanical parameters and greater temperature resistance. In order to use the P-type steels properly and to provide the longest possible time of exploitation, a detailed analysis of material behavior under complex loadings and high temperature should be performed. Structural components made of steel could be subjected to different types of loadings: static tension/torsion, cyclic fatigue, high temperature creep or dynamic loading [5]. High-cyclic fatigue is treated as loading that determines the durability and safety of power plant components working under complex mechanical and high temperature conditions. Therefore, a number of procedures and methods for the quantitative description of the damage degree associated with the impact of mechanical cyclic loads are being developed and applied to enable monitoring of the damage development and its dynamics [6]. Authors investigated damage development under uniaxial loading based on the registration and analysis of material response changes in the form of strain, and cyclic excitation due to stress control. The research program included a selection of specimen geometry and its fastening that prevents buckling during a large number of symmetrical cycles while maintaining constant stress amplitude, as well as registration and analysis of deformation changes in an individual loading cycle. The behavior of power engineering steels subjected to high cycle fatigue (i.e. with a stress amplitude below the yield strength of the material) can be divided in terms of damage development mechanisms into two basic categories. The first one is screening generated by the local deformations around microstructural defects in the form of pores or metallic inclusions. The second mechanism, called cyclic plasticity, is associated with dislocation slips at the level of local sub grains and grains. In both cases, the strain changes measured for the entire specimen volume are the sum of local strain components developing around defects in the case of ratcheting or locally developing slips for cyclic plasticity. Cyclic loading triggers various mechanisms of damage initiation and its further development. In the first group of construction materials, the development of fatigue damage develops around various defects arising in manufacturing processes such as casting or thermal treatment. In the second

*e-mail: mkopec@ippt.pan.pl, m.kopec16@imperial.ac.uk

Manuscript submitted 2021-11-30, revised 2022-02-22, initially accepted for publication 2022-04-12, published in June 2022.

group of metallic materials, plastic flow takes the role of the dominant deformation mechanism that results from the nucleation process, dislocation movement and the activation of slip systems. The entire process of stable damage development develops in accordance with the rules of cyclic plasticity. It should be noticed that fatigue properties of the power engineering steels are determined at room temperature. Because these materials are mainly working at high temperature, it is necessary to provide sufficient data that would allow for full description of P91 steel behavior under aggressive environments, including high temperature and internal pressure. It should be highlighted that in the Polish power plants industry sector, most of the working components made of power engineering steels suffer from high temperature wear and tear exploitation [6]. Such steels are subjected to excessive working under high temperature conditions, and thus their performance should be monitored in order to avoid serious consequences. In order to avoid damage problems due to long term high temperature exposure, proper monitoring of material behavior should be performed in every specific period of time. Such early diagnosis of abnormal states of machinery parts enables industrial plants to avoid heavy economic losses resulting from replacement of damaged machines [7]. The mechanical properties of materials used for specific installations in the power plant sector are determined only on the basis of single-threaded data collected during standard uniaxial tensile tests. However, such tests provide only limited knowledge on material behavior since the data from the test is derived from strain gauge only. Such limitations could be solved by using full-field optical methods, namely electronic speckle pattern interferometry (ESPI) and digital image correlation (DIC) [8]. DIC was found to be an effective tool to ensure the reliability of pressure vessels during service. Although DIC could be used to monitor full-scale components, it has a significantly lower resolution than ESPI [8]. ESPI is the optical technique in which the stress/strain distribution maps can be determined during fatigue testing for a relatively large area of the specimen. ESPI technique is based on holographic interferometry in which the laser beam is distracted from the optically rough surface. Because it is capable to detect cracks in actual and residual stress fields [9], this technique has been widely used to monitor deformation on metallic specimens including steel [8] and aluminum [9] as well as AA2124/SiC metal matrix composites [10] or nickel based superalloys [11]. Hence, it has been found to be a promising tool in stress distribution maps determination for P91 steel specimens tested under different states and in their elastic range. Such maps enable to investigate the effect of long time operation under the power installations conditions on the field strain distributions for each type of specimen.

Therefore, this paper aims to describe in detail the behavior of P91 power plant steel in its elastic range for four different states of material in order to compare their strain/stress distribution maps obtained by means of the ESPI technique. The optical, full-field measurements will provide detailed knowledge on the strain and stress distribution for the as-received and exploited specimens, and thus influence of long time degradation on material integrity will be assessed.

2. MATERIALS AND METHODS

P91 power engineering steel was studied throughout this research. The material of the pipe was certified to confirm the chemical composition presented in Table 1. The hardness of the as-received material was equal to 250HV10. The material was supplied in the form of two pipes with the following dimensions: inner and outer diameter of 78 mm and 90 mm, respectively, and wall thickness of 12 mm. The first one came from a steam pipeline element operated for 80 000 hours at an internal pressure of 8.4 MPa and a temperature of 540°C. The second one was cut off from a new pipeline. The total number of 16 specimens were designed and subsequently produced in the shape and dimensions suitable for full filed ESPI measurements (Fig. 1). A single specimen from each type of material was used to perform a standard tensile test in order to evaluate a set of mechanical properties required to prepare a loading program for subsequent optical measurements. In the next step, two specimens of the material in the as-received state were annealed at the temperature of 200°C for 10 hours in order to reduce residual stress components. Subsequently, they were subjected to fatigue tests at the stress amplitude of 370 MPa, and then stopped at the stage of dynamic growth for the average global strain (measured with an extensometer) in order to introduce a significant degree of damage with a tendency for localization.

Table 1
Chemical composition of P91 steel

Element Wt [%]	C	Si	Mn	P	S	Cr
P91	0.10	0.26	0.48	0.01	0.01	8.43
Mo	Ni	Al	Nb	V	N	Fe
0.90	0.14	0.01	0.07	0.22	0.04	Bal.

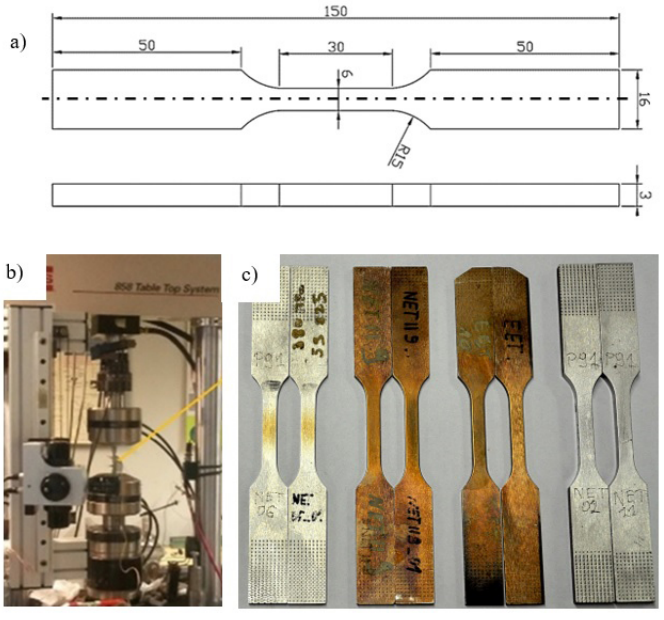

Fig. 1. Experimental details: a) engineering drawing of specimen for fatigue tests; b) experimental setup showing position of the ESPI apparatus; (c) general view of the tested specimens

The specimens manufactured from the exploited pipe were also subjected to annealing (200°C for 10 hours) to reduce residual stress. The detailed list of all specimens used for ESPI measurements was presented in Table 2. Standard uniaxial tensile and fatigue tests were performed on the MTS 858 testing machine. Uniaxial tensile tests were carried out at a strain rate equal to 2×10^{-4} s^{-1}. The fatigue tests were force controlled with zero mean value and constant stress amplitude of 370 MPa with a frequency of 20 Hz. ESPI measurements were performed using the Dantec Dynamics Q100 ESPI system. Microstructural observations and chemical composition analysis were performed using a Jeol J0L6360 LA scanning electron microscope (Jeol, Musashino, Akishima, Tokyo Japan) with an energy dispersive spectroscopy (EDS) attachment (Oxford Instruments, Oxford, United Kingdom).

Table 2
Specimens used for ESPI measurements

No.	Notation	State of material	Heat treatment
1	NP91_1	as-received	–
2	NP91_2	as-received	–
3	NP91_1H	as-received, annealed, after fatigue	200°C, 10 h
4	NP91_2H	as-received, annealed, after fatigue	200°C, 10 h
5	EP91_1	80 000 h exploitation at internal pressure of 8.4 MPa at 540°C	–
6	EP91_2	80 000 h exploitation at internal pressure of 8.4 MPa at 540°C	–
7	EP91_1H	80 000 h exploitation at internal pressure of 8.4 MPa at 540°C, annealed	200°C, 10 h
8	EP91_2H	80 000 h exploitation at internal pressure of 8.4 MPa at 540°C, annealed	200°C, 10 h

3. THEORETICAL BACKGROUND OF ESPI METHOD

Theoretical background of the ESPI methodology is based on the speckle effect. Such an effect occurred during laser beam distraction from the optically rough surface. As a result of radiation scattering on the specimen surface, secondary wave interference occurs. It leads to the formation of characteristic speckle images.

The speckle position and intensity changes during linear and angular displacements of the object are recorded during optical measurement. The fringes can be obtained by the comparison of speckle structures of the undeformed material with the one after deformation. It should be mentioned that during speckle displacement measurements on the specimen surface, the stored frame of the reference structure is continuously subtracted from or added to the dataset obtained at the subsequent measurement.

The experimental procedure was presented in Fig. 2. Firstly, during ESPI measurement, the interference results from the specimen surface are recorded as speckled images using the CCD camera. Subsequently, through the subtraction process of obtained speckle interferograms (before and after loaded up to a particular load value), correlation fringes are generated. The abovementioned phenomena enabled to obtain a phase map that presents the distribution of displacement and average strain components in each direction separately. Finally, the field stress and strain phase maps are determined as a result of mathematical operations with fixed boundary conditions (measurement area dimensions) and material parameters (elastic modulus and Poisson's ratio).

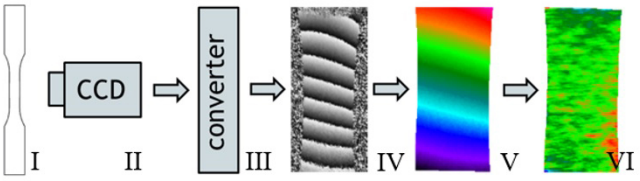

Fig. 2. Experimental procedure of ESPI measurement: recording of interference results from the specimen surface (I) as speckled images using the CCD camera (II) and converter (III); generation of correlation fringes through the subtraction process of obtained speckle interferograms (IV); determination of a phase map presenting the distribution of displacement and average strain components in each direction separately (V) and the field stress and strain phase maps (VI)

In order to obtain strain and stress distribution maps for the plane strain state (1–4) or plane stress state (5–8), the following relationships are used:

$$\varepsilon_n = 0, \tag{1}$$

$$\varepsilon_{1,2} = \frac{\varepsilon_x + \varepsilon_y}{2} \pm \sqrt{\frac{(\varepsilon_{xx} + \varepsilon_{yy})^2}{2} + \left(\frac{\gamma_{xy}}{2}\right)^2}, \tag{2}$$

$$\sigma_{xx} = \frac{E(1-\upsilon)}{(1-2\upsilon)(1+\nu)} \times \left(\varepsilon_{xx} + \frac{\nu}{(1-\nu)}\varepsilon_{yy}\right), \tag{3}$$

$$\sigma_{yy} = \frac{E(1-\upsilon)}{(1-2\upsilon)(1+\nu)} \times \left(\varepsilon_{yy} + \frac{\nu}{(1-\nu)}\varepsilon_{xx}\right), \tag{4}$$

$$\sigma_n = 0, \tag{5}$$

$$\sigma_{xx} = \frac{E}{(1-\upsilon^2)} \times (\varepsilon_{xx} + \nu \times \varepsilon_{yy}), \tag{6}$$

$$\sigma_{yy} = \frac{E}{(1-\upsilon^2)} \times (\varepsilon_{yy} + \nu \times \varepsilon_{xx}), \tag{7}$$

$$\sigma_{1,2} = \frac{\sigma_{xx} + \sigma_{yy}}{2} \pm \sqrt{\frac{(\sigma_{xx} + \sigma_{yy})^2}{2} + (\tau)^2}. \tag{8}$$

4. RESULTS AND DISCUSSION

4.1. Microstructural characterization and mechanical properties

The microstructure of P91 steel specimens in as-received and the post-operational state consists of needle shaped tempered martensite with carbide secretions (Fig. 3). The P91 steel in as-received condition was characterized by higher homogeneity

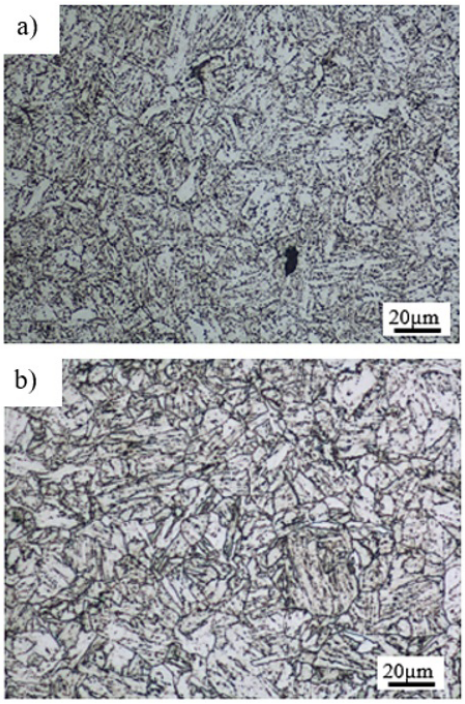

Fig. 3. Microstructure of P91 steel in as-received condition (a) and after 80 000 h of exploitation (b)

in structure and smaller grain size in comparison to the coarse structure of post-operational material.

Selected mechanical properties of P91 steel in the as-received state and after exploitation were determined based on standard tensile tests (Fig. 4). In order to obtain reliable results, three specimens were tested accordingly. The average values of parameters determined from these tests are presented in Table 3.

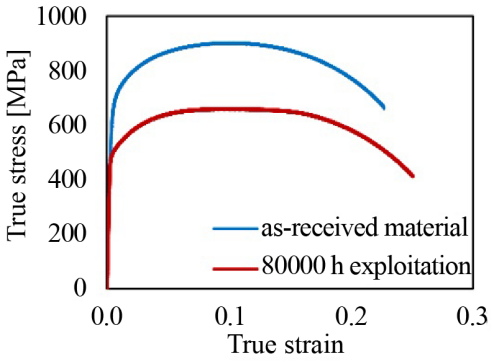

Fig. 4. Tensile characteristics of P91 steel

Table 3

Mechanical properties of P91 steel in the as-received state, after 80 000 h of exploitation and according to the Polish Standards

	R_m [MPa]	R_e [MPa]	A [%]
As-received	903 (±7)	661 (±5)	23 (±0.2)
80 000 h exploitation	662 (±6)	497 (±5)	24.5 (±0.2)
PN: 10216-2:2004	630–830	> 450	17–19

4.2. Strain fields mapping

Assessments of the field stress components distributions were based on the strain field measurements using the ESPI camera. The specimen loading program was carried out in five steps from 0 to 2.5 kN. The loading step of 500 N corresponded to the maximum force, which allowed to maintain a stability of the interference fringes during optical measurements. The total strain was measured using an MTS longitudinal extensometer with a gauge length of 30 mm. The strain maps of all measured specimens in the loading direction were presented in Fig. 5. The exploited specimens exhibit a similar character of the deformation development as the as-received ones in the same specific loading range from 0 to 2.5 kN. Homogeneous strain distribution over the entire surface of the gauge part of the specimen was observed. The variations of measured values do not exceed 0.035%. The results obtained from ESPI were also presented in the form of strain profiles along the symmetry axis (Fig. 6). It should be noticed that relatively low strain values were observed near the grips in which the specimens were clamped. A relatively uniform strain distribution ranging from 0.20 to 0.25×10^{-3} was observed for all specimens in the central area found between 5 and 25 mm of the gauge length.

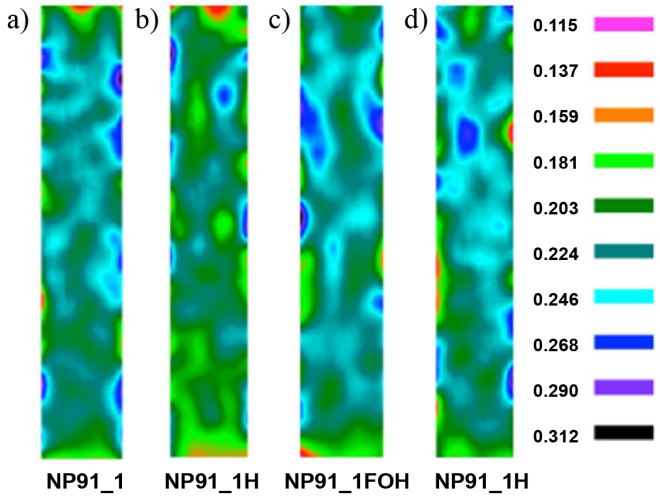

Fig. 5. Distribution of strain fields for the as-received specimen (a); annealed as-received specimen after fatigue (b); exploited specimen (c) and annealed exploited specimen (d)

The NP91_1 specimen represented P91 steel in the as-received state, without any loading history. The strain distribution on the specimen surface was homogeneous, without visible strain accumulation and damage initiation (NP91_1). ESPI measurements for specimen NP91_1H, representing the annealed material (P91 steel) after fatigue, exhibited a similar level of average strain as that for the as-received material observed, however with some smaller variation of values (NP91_1H). The maximum difference in strain values for the as-received specimens was approx. 0.061%, while for the annealed state this value reached only 0.018%. Specimens of P91 steel after long-term operation, subjected to annealing at the temperature of 200°C, exhibited the lowest strain level in the range of up to 0.08% (NP91_1FOH and NP91_1H).

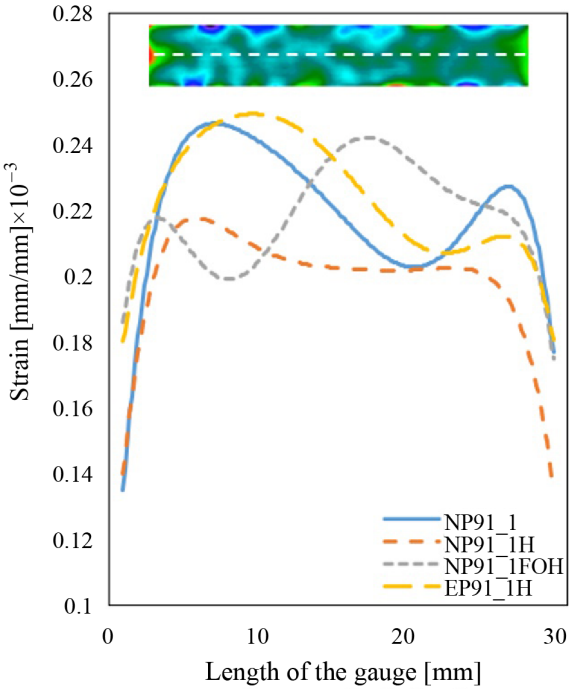

Fig. 6. Strain profiles across the gauge length

Such results were comparable with the deformation degree of the as-received specimens after annealing. Figure 7 presents a summary of the ESPI measurements obtained for all specimens. It is worth mentioning that the strain values captured from the extensometer measurements were slightly higher for almost all specimens tested. This could be explained by a slightly smaller gauge area for the ESPI measurements. The ESPI measurements covered the area marked by a frame, which was within the area limited by the extensometer gauge length in order to maintain accuracy. Both measurement techniques, applied during the loading up of to 2.5 kN, gave a strain level of approx. 0.7% for all specimens in question. Such result leads to the conclusion that long-term operation did not change the mechanical response of P91 steel in its elastic range in comparison to the material without prior loading history. The strain distribution maps are similar without any clear heterogeneities on the specimen surface. Optical measurements did not reveal any areas of potential cracking.

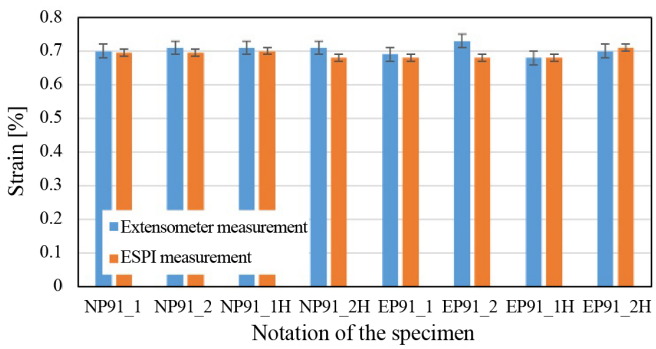

Fig. 7. Comparison of the strain response measured by the extensometer and ESPI method

4.3. Stress fields mapping

Based on the strain maps, stress maps were determined for all types of specimens. The results indicate the homogeneity of stress distribution along the tensile direction in the range of the applied force equal to 2.5 kN for all specimens. The distribution of the stress values for individual specimens is shown in Fig. 8. Although the strain maps for all specimens exhibited homogenous distribution of about 0.7%, the stress maps are different for each condition. Such effect can be attributed to a relatively uniform stress increase over the entire measuring area. The as-received specimen was characterized by uniform stress distribution of about 155 MPa observed on its surface (NP91_1). It should be highlighted that the heat treatment process performed on the as-received specimen enabled a reduction of the stress distribution to about 140 MPa (NP91_1H). A similar reduction was also observed for the exploited specimen, in which stress of approx. 165 MPa was found as slightly lower and equal to 155 MPa (NP91_1FOH and NP91_1H). The effect of long-term exploitation on the stress distribution of P91 steel was observed thanks to the ESPI method. The P91 steel operated for 80 000 hours at internal pressure of 8.4 MPa and temperature of 540°C exhibited a significant stress increase over the entire gauge. The results presented in the form of stress distribution maps were also presented as stress profiles in the symmetry axis of each specimen (Fig. 9). The as-received specimens marked as NP91_1 and NP91_1H were characterized by relatively uniform stress distribution of 145–152 MPa in the central part of the gauge length. Variations of stress distribution were observed for specimens obtained from the exploited pipe, where stress fluctuations are considerable. It should be highlighted that the differences in both strain and stress distribution for all specimens near the specimen clamping area are related to errors resulting from edge effects that are commonly observed during ESPI measurements. The accumulation of stress on the specimen edges is one of many reasons why ESPI is used to investigate damage accumulation near holes [12] and notches [13].

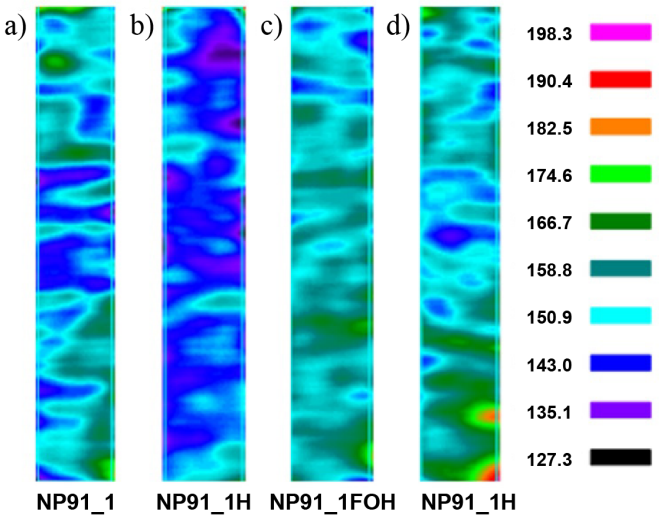

Fig. 8. Distribution of stress fields for the as-received specimen (a); annealed as-received specimen after fatigue (b); exploited specimen (c) and annealed exploited specimen (d)

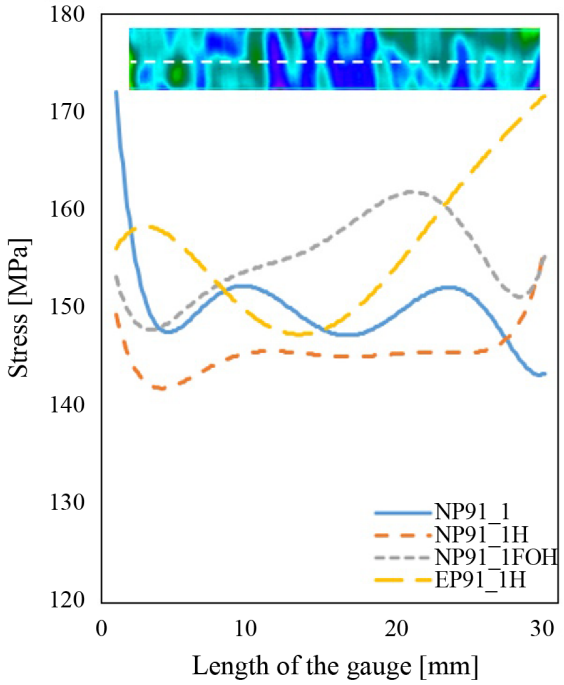

Fig. 9. Stress profiles across the gauge length

ESPI method was also used to compare the Young's modulus measurements of different states of material to those obtained from an extensometer. As it was observed in Fig. 10, the extensometer-based calculations of the elastic modulus always provided its higher value. This is probably caused by the size of the gauge area on which the extensometer is recording major strain changes.

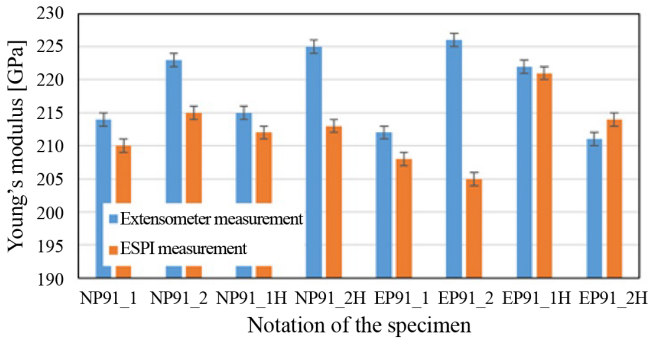

Fig. 10. Comparison of the Young's modulus determined using data captured by the extensometer and ESPI method

The results obtained from such extensometer gauge provide average strain values from limited strain gauge. On the other hand, ESPI can monitor the specimen surface and subsequently obtain displacement maps during its loading. It should be mentioned that ESPI was reported as an effective tool for both Young's modulus and Poisson's ratio evaluation. Michtchenko [14] used the ESPI method to compare the calculated and experimentally captured values of strain. The differences observed for aluminum, copper and brass measurements were within 5%.

In the Polish power plant sector, most of the structural components made of energetic steel gradually lose their initial mechanical properties due to high temperature exposure and subsequent wear leading to degradation of the material during exploitation [5]. In order to avoid the issues related to damage caused by prolonged high temperature operation, material behavior should be carefully monitored over certain periods of time. The combination of destructive mechanical tests and non-destructive ESPI technique will allow to further expand the knowledge on predicting structural components' damage development in their critical wear state. It should be noted that the mechanical properties of materials used in specific power plant installations are determined based on the unit data collected during standard uniaxial tensile tests only. This method provides only limited data by which material behavior can be described and predicted inaccurately. The proposed methodology is therefore very important for the safe operation of transmission systems, machinery and equipment operating at high temperatures and under complex stress conditions, with particular emphasis on pre-critical situations. The listed structural elements made of power steel can be subjected to various types of loads: static compression / tension, cyclic loads, creeping load at high temperature or dynamic load. Therefore, a number of procedures and methods are being developed to monitor damage development and its dynamics. Unfortunately, the available data from the literature review do not allow to fully understand the mechanisms of damage and degradation of power engineering steels subjected to high temperatures and complex stress. The methodology presented in this work could serve as an effective indicator of the damage since the strain and stress distribution maps for each condition of the material could be compared to the as-received state and failure of the material could therefore be avoided.

5. CONCLUSIONS

The main concluding remarks are presented below:

1. The ESPI methodology for full-field stress distribution measurements enables to assess homogeneity of the strain and stress distributions of the tested material as a function of the loading applied.
2. Such method provided detailed information on the area tested, and thus was found to be more effective than the conventional extensometer technique in terms of material integrity monitoring.
3. ESPI measurements exhibited a lack of any visible effects on the strain distribution maps related to long-term loading of specimens operation under power installations conditions for specimens loaded with up to 2.5 kN, i.e. forces corresponding to real conditions in power plants. It was concluded that the ESPI technique could be effectively used to monitor the degradation degree in power engineering steels.

ACKNOWLEDGEMENTS

The author would also like to express his gratitude to the technical staff – Mr. M. Wyszkowski and Mr. A. Chojnacki for their kind help during the experimental part of this work.

This work has been partially supported by the National Science Centre through Grant No. 2019/35/B/ST8/03151.

REFERENCES

[1] D. Kukla, Z.L. Kowalewski, P. Grzywna, and K. Kubiak, "Assessment of fatigue damage development in power engineering steel by local strain analysis", *Kov. Mater.,* vol. 52, pp. 269–277, 2014, doi: 10.4149/km_2014_5_269.

[2] G. Junak and M. Cieśla, "Low-cycle fatigue of P91 and P92 steels used in the power engineering industry", *Arch. Mater. Sci. Eng.*, vol. 48, pp. 19–24, 2011.

[3] A. Sedmak, M. Swei, and B. Petrovski, "Creep crack growth properties of P91 and P22 welded joints", *Fatigue Fract. Eng. Mater. Struct.,* vol. 40, pp. 1267–1275, 2017, doi: 10.1111/ffe.12628.

[4] A. Zieliński, *Trwałość eksploatacyjna żarowytrzymałych stali o osnowie ferrytycznej w warunkach długotrwałego oddziaływania temperatury (Service life of heat-resistant ferrite matrix steels under long-term temperature exposure)*, Gliwice: Instytut Metalurgii Żelaza im. Stanisława Staszica, 2016, pp. 1–198.

[5] T. Siwowski, "Fatigue assessment of existing riveted truss bridges: case study", *Bull. Pol. Acad. Sci. Tech. Sci.*, vol. 63, no. 1, pp. 125–133, 2015, doi: 10.1515/bpasts-2015-0014.

[6] M. Kopec, D. Kukla, A. Brodecki, and Z.L. Kowalewski, "Effect of high temperature exposure on the fatigue damage development of X10CrMoVNb9-1 steel for power plant pipes", *Int. J. Press. Vessel. Pip.*, vol. 189, pp. 104282-1–16, 2021, doi: 10.1016/j.ijpvp.2020.104282.

[7] A. Głowacz, and Z. Głowacz, "Recognition of rotor damages in a DC motor using acoustic signals", *Bull. Pol. Acad. Sci. Tech. Sci.*, vol. 65, no. 2, pp. 187–194, 2017, doi: 0.1515/bpasts-2017-0023.

[8] M. Kopec, D. Kukla, A. Brodecki, and Z.L. Kowalewski, "Suitability of DIC and ESPI optical methods for monitoring fatigue damage development in X10CrMoVNb9-1 power engineering steel", *Arch. Civ. Mech.*, vol. 21, pp. 167-1–13, 2021, doi: 10.1007/s43452-021-00316-1.

[9] T. Sasaki, S. Hasegawa, and S. Yoshida, "Fatigue Damage Analysis of Aluminum Alloy by ESPI – Residual Stress, Thermomechanics & Infrared Imaging, Hybrid Techniques and Inverse Problems" in *Conference Proceedings of the Society For Experimental Mechanics Series*, 2016, pp. 147–154, doi: 10.1007/978-3-319-21765-9_19.

[10] A. Rutecka, P. Grzywna, and L. Dietrich, "Damage Detection of AA2124/SiC Metal Matrix Composites Using Electronic Speckle Pattern Interferometry", *Solid State Phenom.*, vol. 240, pp. 122–127, 2016, doi: 10.4028/www.scientific.net/ SSP.240.122.

[11] M. Kopec, P. Grzywna, D. Kukla, and Z.L. Kowalewski, "Evaluation of the fatigue damage development using ESPI method", *Inżynieria Materiałowa*, vol. 212, pp. 201–205, 2016, doi: 10.15199/28.2016.4.9.

[12] Y. Matvienko, V. Pisarev, and S. Eleonsky, "The effect of low-cycle fatigue parameters on damage accumulation near a hole", *Eng. Fail. Anal.*, vol. 106, pp. 1–19, 2019, doi: 10.1016/j.engfailanal.2019.104175.

[13] Y. Matvienko, V. Pisarev, and S. Eleonsky, "Investigation of fatigue damage accumulation by measurements of deformation response to narrow notch increment", *Procedia Struct. Integr.*, vol. 28, pp. 584–590, 2020, doi: 10.1016/j.prostr.2020.10.068.

[14] A. Michtchenko, "Application of Electronic Speckle Pattern Interferometry Method for Simultaneous Measurement of Young's Modulus and the Poisson's Ratio of Metals", *Proceedings*, vol. 2, pp. 521-1–7, 2018, doi: 10.3390/ICEM18-0539.